

## Optical model calculations on the threshold anomaly for the ${}^6\text{Li} + {}^{28}\text{Si}$ and ${}^7\text{Li} + {}^{28}\text{Si}$ systems at near-Coulomb-barrier energies

A. Gómez Camacho,<sup>1</sup> P. R. S. Gomes,<sup>2</sup> and J. Lubian<sup>2</sup><sup>1</sup>*Departamento de Aceleradores, Instituto Nacional de Investigaciones Nucleares, Apartado Postal 18-1027, C.P. 11801, México, D.F., Mexico*<sup>2</sup>*Instituto de Física, Universidade Federal Fluminense, Avenida Litoranea s/n, Gragoatá, Niterói, Rio de Janeiro 24210-340, Brazil*

(Received 12 October 2010; revised manuscript received 17 November 2010; published 17 December 2010)

A simultaneous analysis of elastic scattering, fusion, and total reaction cross sections for the weakly bound systems  ${}^6,7\text{Li} + {}^{28}\text{Si}$  at energies close to the Coulomb barrier is performed by optical model calculations. The nuclear polarization potential  $U$  is split into volume part  $U_F$ , which accounts for fusion reactions and a surface part  $U_{DR}$ , responsible for direct reactions. The parameters of the Woods-Saxon potentials are determined by a  $\chi^2$  analysis of the data. The presence of the threshold anomaly or the breakup threshold anomaly is investigated from the energy dependence of both the fusion and direct reaction parts of the polarization potential.

DOI: 10.1103/PhysRevC.82.067601

PACS number(s): 25.70.Bc, 24.10.Ht, 27.30.+t

For some time it has been known that reactions with heavy systems present the so-called threshold anomaly (TA), i.e., the real and imaginary parts of the optical potential obtained from elastic scattering fits around the Coulomb barrier, and show a distinctive energy dependent behavior. The imaginary potential drops sharply as the energy decreases toward the barrier energy, while the real potential strength shows a strong localized peak around the barrier. At higher energies both potentials are almost energy independent [1]. This energy behavior of the optical potential is understood in terms of the strong coupling between the elastic scattering channel to other reaction channels that produce an attractive polarization potential. The absolute value of this attractive real polarization potential increases the strength of the already attractive nuclear potential which, in turn, lowers the fusion barrier and consequently produces an enhancement of the fusion cross sections at energies below the Coulomb barrier. This energy dependence of the real potential is expressed frequently by

$$V(E) = V_0 + \Delta V(E), \quad (1)$$

where  $V_0$  is the real nuclear potential at high energies and  $\Delta V(E)$  the polarization potential. The decrease of the imaginary potential  $W(E)$  of the optical potential as the collision energy approaches the barrier is due to the closing of reaction channels. It is also well known that the energy dependence between the real and imaginary polarization potentials are connected by the dispersion relation expressed by the principal integral value [2],

$$\Delta V(E) = \frac{\mathbf{P}}{\pi} \int_{-\infty}^{+\infty} \frac{W(E')}{E' - E} dE'. \quad (2)$$

It is then clear that any strong change in  $W(E)$  must be accompanied by a localized strong variation in  $\Delta V(E)$ . In the case where weakly bound projectiles are involved, many studies reveal that the situation is quite different. Due to the weak binding energy of the nucleus, strong couplings between breakup and elastic channels at energies below the Coulomb barrier may arise. In such a situation, the imaginary part  $W(E)$  of the optical potential cannot sharply decrease, as it does for tightly bound nuclei, since it must account for the appreciable

breakup cross-section yields observed at energies below the barrier. Accordingly, the real part of the polarization potential  $\Delta V(E)$  does not contribute to an increase in the strength of the nuclear potential, but instead has a repulsive characteristic. This new phenomenon has been termed the breakup threshold anomaly (BTA) [3]. Based on their measured transfer cross section much higher than the breakup cross section at the near barrier energy for the  ${}^6,7\text{Li} + {}^{28}\text{Si}$  system, Pakou *et al.* [4–8] argue that transfer channels can also be important at low energies for some weakly bound systems, and therefore those channels may be the main reason for the nondecreasing of the imaginary potential at near barrier energies. The BTA has been investigated in a large number of nuclear systems involving weakly bound projectiles with a variety of medium and large mass targets, for instance  ${}^9\text{Be}$  with  ${}^{27}\text{Al}$  [9], with  ${}^{64}\text{Zn}$  [10–13], with  ${}^{144}\text{Sm}$  [14,15] and with  ${}^{208}\text{Pb}$ ,  ${}^{209}\text{Bi}$  [16,17];  ${}^6\text{Li}$  and  ${}^7\text{Li}$  with targets  ${}^{208}\text{Pb}$  [3,18],  ${}^{27}\text{Al}$  [19–21],  ${}^{144}\text{Sm}$  [22],  ${}^{58,64}\text{Ni}$  [23,24],  ${}^{59}\text{Co}$  [25],  ${}^{90}\text{Zr}$  [26],  ${}^{138}\text{Ba}$  [11,27,28],  ${}^{28}\text{Si}$  [6]. Although the BTA is observed in all systems involving  ${}^6\text{Li}$ , for  ${}^7\text{Li}$  its presence is observed for some systems but not for others. The reason may probably be due to the competition between the attractive polarization potential due to the bound excited state of  ${}^7\text{Li}$  [28] and the repulsive breakup polarization potential [29]. The BTA has also been observed in some neutron and proton radioactive halo nuclei such as,  ${}^6\text{He}$  with  ${}^{209}\text{Bi}$  [30] and  ${}^8\text{B}$  with  ${}^{58}\text{Ni}$  [24,31].

Several optical model potentials have been used to describe elastic scattering data for the systems cited above, as for example, double folding potentials. Woods-Saxon potentials with volume and surface parts have also been applied to the simultaneous description of fusion and elastic scattering data of various systems [14,24,32]. In this case, the volume potential is defined as responsible for fusion reactions whereas the surface part is responsible for direct reactions, including breakup and transfer processes.

It is the aim of the present work to show the results of calculations performed for the systems  ${}^6,7\text{Li}$  on the target  ${}^{28}\text{Si}$ , obtained when such a simultaneous description of fusion and elastic scattering data is looked for. The parameters of the fusion  $U_F$  (volume) are determined in such a way that fusion cross-section data  $\sigma_F$  are fitted, while those of the

direct reaction potential  $U_{DR}$  (surface) are found from the fit to direct reaction cross sections  $\sigma_{DR} = \sigma_T - \sigma_F$ , where  $\sigma_T$  is the total reaction cross section.  $\sigma_T$  is calculated from the total absorption imaginary potential  $W_T = W_F + W_{DR}$ , that is,

$$\sigma_i = (2/\hbar v) \langle \chi^{(+)} | W_i | \chi^{(*)} \rangle, \quad i = T, F, DR, \quad (3)$$

where  $\chi^{(+)}$  is the solution of  $[T + \mathcal{V}]\chi^{(+)} = E\chi^{(+)}$ ,  $\mathcal{V} = V_{Coul} - (V_0 + U)$ , and  $V_0$  is the energy independent nuclear Hartree-Fock potential,  $U$  represents the polarization potential  $U = U_F + U_{DR}$  with  $U_F = V_F + iW_F$  and  $U_{DR} = V_{DR} + iW_{DR}$ . The real parts  $V_F$ ,  $V_{DR}$  and the imaginary parts  $W_F$ ,  $W_{DR}$  are correspondingly connected by the dispersion relation. This approach has been applied to a large number of tightly and weakly bound systems and a more extensive description of it is given in Refs. [24,32,33]. The energy behavior of  $U_F$  and  $U_{DR}$ , that is of  $V_F$ ,  $W_F$ ,  $V_{DR}$ , and  $W_{DR}$ , can thus be obtained and the presence of either the TA or BTA can be inferred as the collision energy approaches the barrier. Simultaneous fits to elastic scattering, fusion, and total reaction cross-section data are then performed to extract the optical potential parameters of the fusion and direct reaction potentials.

For the system  ${}^6\text{Li} + {}^{28}\text{Si}$ , elastic scattering measurements by Pakou *et al.* [4] at the near barrier energies  $E_{lab} = 7.5, 9, 11$ , and 13 MeV have been used, while at higher energies,  $E_{lab} = 20, 27$ , and 30 MeV, we used data from Refs. [34–36]. For fusion cross sections  $\sigma_F$ , the recent sub- and above-barrier measurements of Sinha *et al.* were used [37]. The total reaction cross sections  $\sigma_T$  are those from Refs. [5,38]. For  ${}^7\text{Li} + {}^{28}\text{Si}$ , elastic scattering, fusion and total reaction cross section data are those of Refs. [6,39,40] and [5,7], respectively. In the simultaneous fitting calculations, we used fixed diffuseness and reduced radii for the fusion and direct reaction potentials for all energies:  $a_F = 0.6$  fm,  $r_F = 1.4$  fm,  $a_{DR} = 0.6$  fm, and  $r_{DR} = 1.6$  fm for  ${}^6\text{Li} + {}^{28}\text{Si}$  and  $a_F = 0.6$  fm,  $r_F = 1.4$  fm,  $a_{DR} = 0.7$  fm, and  $r_{DR} = 1.6$  fm for  ${}^7\text{Li} + {}^{28}\text{Si}$ . As described in Refs. [14,24,32], the real  $V_F$  and imaginary  $W_F$  parts of the Woods-Saxon fusion polarization potential  $U_F$  are assumed to have the same geometric volume shape, with the same diffuseness and reduced radius. On the other hand, the corresponding direct reaction real and imaginary polarization potentials  $V_{DR}$  and  $W_{DR}$  of  $U_{DR}$  have the same surface geometric shape, with the same diffuseness and reduced radius. So, only the strengths  $V_F(E)$ ,  $W_F(E)$ ,  $V_{DR}(E)$ , and  $W_{DR}(E)$  are the variables to be obtained in the simultaneous  $\chi^2$  analysis of the data.

In Figs. 1 and 2, the results for the fusion and direct reaction potential strengths that fit elastic scattering, fusion and total reaction data for  ${}^6\text{Li} + {}^{28}\text{Si}$  and  ${}^7\text{Li} + {}^{28}\text{Si}$  are shown. As can be seen from these figures, for both systems, as the collision energy approaches the corresponding barrier energy  $V_B$ , the energy variation of the absorption fusion potentials  $W_F(E)$  decreases even above the barrier, while the real counterparts  $V_F(E)$  have an increasing behavior. This is a signature that the TA is present for the fusion potentials. On the other hand, the surface potential strengths  $W_{DR}(E)$  and  $V_{DR}(E)$  show an energy behavior compatible with the BTA for both systems, although it is much more clear for the  ${}^6\text{Li} + {}^{28}\text{Si}$

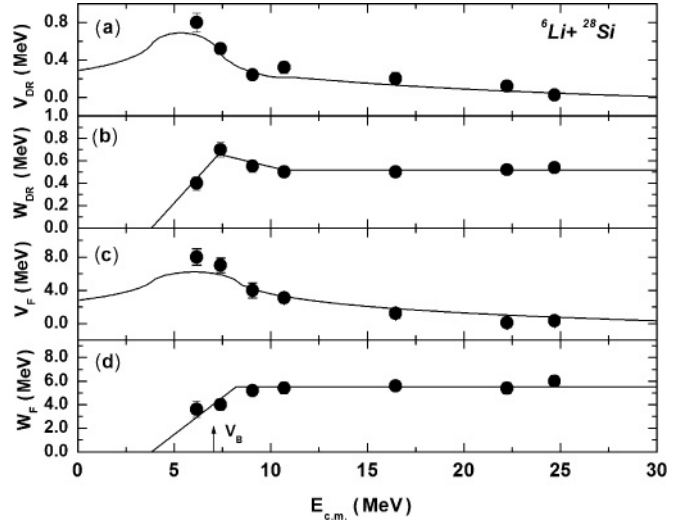


FIG. 1. Strengths for direct reaction and fusion potentials as obtained from the simultaneous  $\chi^2$  analysis of elastic scattering, fusion and total reaction cross-section data for  ${}^6\text{Li} + {}^{28}\text{Si}$ .

system than for  ${}^7\text{Li} + {}^{28}\text{Si}$ , probably due to the reasons that we have mentioned above. For both systems,  $W_{DR}(E)$  does not decrease above the barrier as the bombarding energy decreases toward the barrier. On the contrary, there is a slight increase of  $W_{DR}(E)$  at the barrier energy region. The decrease of  $W_{DR}(E)$  starts only at energies below the barrier. For  ${}^6\text{Li} + {}^{28}\text{Si}$ , the lines shown in Figs. 1(b) and 1(d) were used to fit the  $W_{DR}(E)$  and  $W_F(E)$  values and also to integrate the energy scaled dispersion relation [2],

$$V_i(E) = V_i(E_{s,i}) + (E - E_{s,i}) \frac{1}{\pi} \mathcal{P} \times \int_0^\infty \frac{W_i(E')}{(E' - E_{s,i})(E' - E)} dE', \quad i = F, DR, \quad (4)$$

the results are shown by the lines in Figs. 1(a) and 1(c), respectively. For the direct reaction potential, the reference

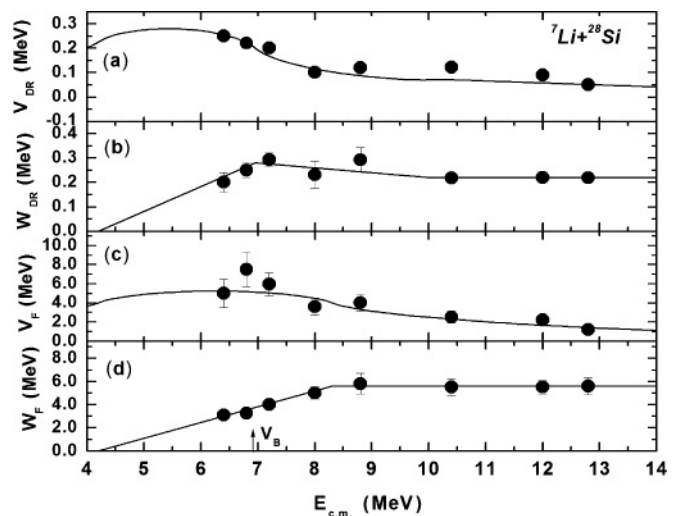


FIG. 2. Same as Fig. 1 for the  ${}^7\text{Li} + {}^{28}\text{Si}$  system.

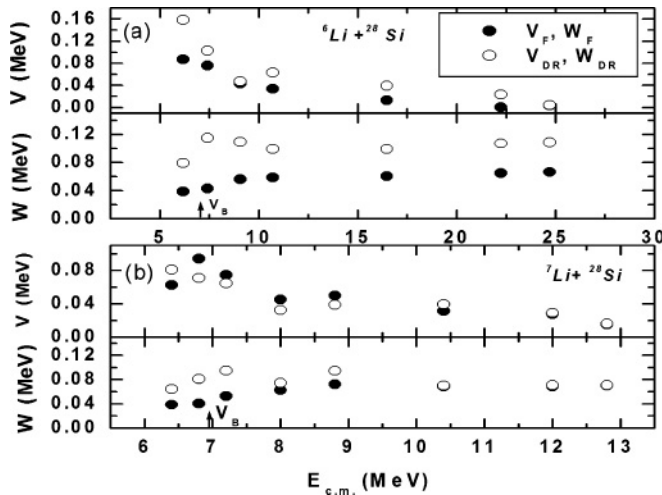


FIG. 3. Energy dependence of the fusion and direct reaction real  $V$  and imaginary  $W$  parts of the polarization potentials at the corresponding strong absorption radius  $R_{sa}$  for (a)  ${}^6\text{Li} + {}^{28}\text{Si}$  and (b)  ${}^7\text{Li} + {}^{28}\text{Si}$ .

value of the potential is set at  $V_{DR}(E_{s,DR}) = 0.5$  MeV, at the reference energy  $E_{s,DR} = 7.3$  MeV, while for the fusion potential,  $V_F(E_{s,F}) = 5.0$  MeV at  $E_{s,F} = 8.2$  MeV. Similarly, for the  ${}^7\text{Li} + {}^{28}\text{Si}$  system, the results are shown in Fig. 2, where  $V_{DR}(E_{s,DR}) = 0.2$  MeV at  $E_{s,DR} = 6.95$  MeV and  $V_F(E_{s,F}) = 4.0$  MeV at  $E_{s,F} = 8.3$  MeV. As observed in Figs. 1(a), 1(c), 2(a), and 2(c), the values of the direct reaction  $V_{DR}(E)$  and fusion  $V_F(E)$  potential strengths obtained from the simultaneous fit of the elastic, direct reaction, and fusion data are close to those values predicted by the dispersion relation.

It is interesting to notice that since the diffuseness parameters  $a_F$  and  $a_{DR}$  and reduced radii  $r_F$  and  $r_{DR}$  of the potentials are kept constant at all energies for both nuclear systems, the same energy behavior for the potential strengths shown in Figs. 1 and 2 is obtained for the radial dependent volume and surface geometric functions  $V_{DR}(E, r)$ ,  $W_{DR}(E, r)$ ,  $V_F(E, r)$ , and  $W_F(E, r)$ , when these are evaluated at the strong absorption radius  $R_{sa}$ . This is illustrated in Fig. 3, where also it is observed that  $|W_F(E, R_{sa})| < |W_{DR}(E, R_{sa})|$  at all energies. That is, direct reactions dominate over fusion ones, particularly as the energy approaches the barrier energy  $V_B$ . As claimed by Pakou *et al.* [4–8], direct reactions are not just breakup processes, but also transfer channels, which may even be more important than breakup at some energies for these systems.

The results of the simultaneous fits for the elastic scattering angular distributions for both systems are excellent. They are not shown in this Brief Report due to the limits of the length of this paper. The calculated values for fusion cross sections  $\sigma_F$  are shown in Fig. 4 for both systems. Reaction cross sections  $\sigma_T$  are shown in Fig. 5. For those energies where elastic scattering measurements are available but fusion data were not explicitly measured, we assumed those values obtained from a Wong fitting to the existing data [41]. Similarly, for those energies where reaction cross sections are not directly measured, we considered those values extracted from the corresponding elastic scattering data.

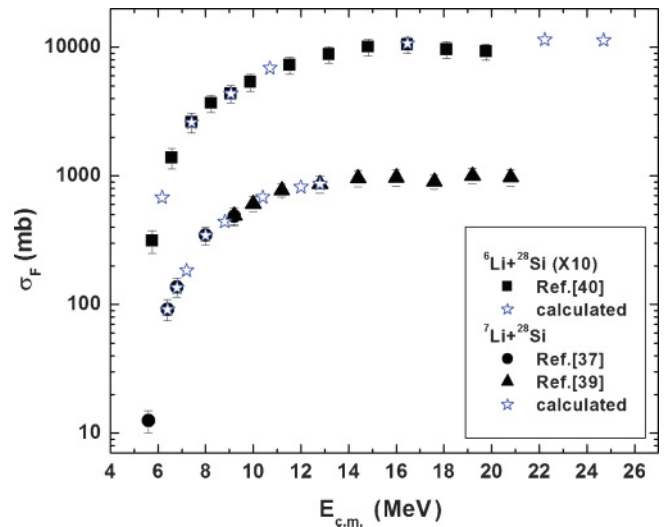


FIG. 4. (Color online) Calculated fusion cross-section values as obtained from the simultaneous  $\chi^2$  analysis. To distinguish the systems, those values corresponding to  ${}^6\text{Li} + {}^{28}\text{Si}$  have been multiplied by 10.

In conclusion, from the results of the present work, the conjugated effects for the energy dependence of the polarization potentials indicate that the systems  ${}^6\text{Li} + {}^{28}\text{Si}$  and  ${}^7\text{Li} + {}^{28}\text{Si}$  present the so-called breakup threshold anomaly. This phenomenon is more clearly observed for the  ${}^6\text{Li} + {}^{28}\text{Si}$  system than for  ${}^7\text{Li} + {}^{28}\text{Si}$ . It is observed that at  $R_{sa}$ , direct reaction potentials dominate over fusion ones at all energies, particularly as the energy approaches the barrier. This is in agreement with the fact that direct reactions, particularly breakup and/or transfer cross sections, are important and nonvanishing at energies below the barrier energy. The simultaneous  $\chi^2$  analysis of the data for both systems  ${}^6\text{Li} + {}^{28}\text{Si}$  and  ${}^7\text{Li} + {}^{28}\text{Si}$  are in close agreement to the data. We have shown very clearly that the method of separating the optical potential into fusion and direct reaction potentials is a powerful tool to

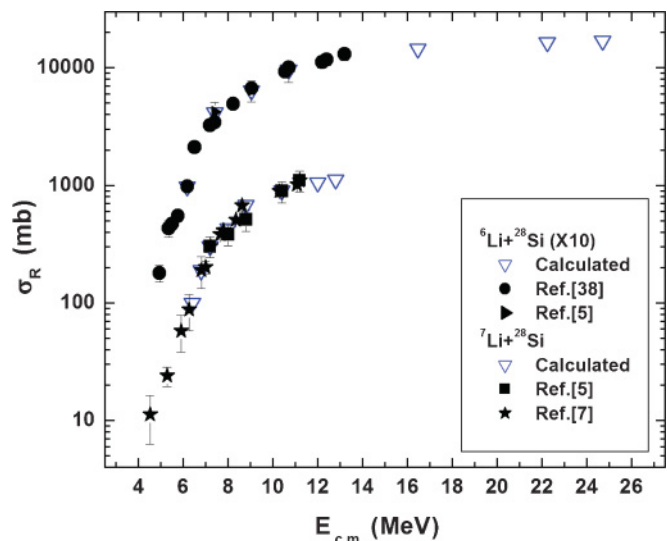


FIG. 5. (Color online) Same as Fig. 4 for reaction cross sections.

disentangle the opposite effects of production of attractive and repulsive polarization potentials by different reaction mechanisms. The two combining effects may lead to different net effects on the energy dependence of the total optical potential of different combinations of projectiles and targets.

Finally, it is important to mention that a very recent and interesting work by Zerva *et al.* [42] investigated the behavior of the optical potentials for these same systems by the alternative method of measuring quasielastic backscattering and deriving the corresponding barrier distribution. In that paper it is found that for the  ${}^6\text{Li} + {}^{28}\text{Si}$  system the optical

potential follows the dispersion relation, as we found in the present work, but for the  ${}^7\text{Li} + {}^{28}\text{Si}$  system the dispersion relation is not satisfied, contrary to our conclusions. From both works and others in literature, one observes that the behavior of the optical potential for the scattering of  ${}^6\text{Li}$  is, at present, much better understood than for  ${}^7\text{Li}$ . Further investigation is required for a deeper understanding of the scattering of the  ${}^7\text{Li}$  nucleus.

P.R.S.G. and J.L. acknowledge the financial support from CNPq, PRONEX, and FAPERJ.

- 
- [1] G. R. Satchler, *Nucl. Phys. A* **472**, 591 (1987).  
 [2] C. Mahaux, H. Ngô, and G. R. Satchler, *Nucl. Phys. A* **449**, 354 (1986).  
 [3] M. S. Hussein, P. R. S. Gomes, J. Lubian, and L. C. Chamon, *Phys. Rev. C* **73**, 044610 (2006).  
 [4] A. Pakou *et al.*, *Phys. Lett. B* **556**, 21 (2003).  
 [5] A. Pakou *et al.*, *Nucl. Phys. A* **784**, 13 (2007).  
 [6] A. Pakou *et al.*, *Phys. Rev. C* **69**, 054602 (2004).  
 [7] A. Pakou *et al.*, *Eur. Phys. J. A* **39**, 187 (2009).  
 [8] A. Pakou *et al.*, *Phys. Rev. Lett.* **90**, 202701 (2003); *Phys. Rev. C* **71**, 064602 (2005); *Phys. Lett. B* **633**, 691 (2006); *Phys. Rev. C* **76**, 054601 (2007); A. Pakou, *ibid.* **78**, 067601 (2008).  
 [9] P. R. S. Gomes *et al.*, *Phys. Rev. C* **70**, 054605 (2004).  
 [10] P. R. S. Gomes *et al.*, *Phys. Rev. C* **71**, 034608 (2005).  
 [11] P. R. S. Gomes *et al.*, *J. Phys. G* **31**, S1669 (2005).  
 [12] S. B. Moraes *et al.*, *Phys. Rev. C* **61**, 064608 (2000).  
 [13] M. Zadro *et al.*, *Phys. Rev. C* **80**, 064610 (2009).  
 [14] A. Gómez Camacho, P. R. S. Gomes, J. Lubian, E. F. Aguilera, and I. Padron, *Phys. Rev. C* **76**, 044609 (2007).  
 [15] P. R. S. Gomes *et al.*, *Nucl. Phys. A* **828**, 233 (2009).  
 [16] C. Signorini *et al.*, *Phys. Rev. C* **61**, 061603(R) (2000).  
 [17] R. J. Woolliscroft *et al.*, *Phys. Rev. C* **68**, 014611 (2003).  
 [18] N. Keeley *et al.*, *Nucl. Phys. A* **571**, 326 (1994).  
 [19] J. M. Figueira *et al.*, *Phys. Rev. C* **75**, 017602 (2007).  
 [20] J. O. Fernandez Niello *et al.*, *Nucl. Phys. A* **787**, 484 (2007).  
 [21] J. M. Figueira *et al.*, *Phys. Rev. C* **73**, 054603 (2006).  
 [22] J. M. Figueira *et al.*, *Phys. Rev. C* **81**, 024613 (2010).  
 [23] M. Biswas *et al.*, *Nucl. Phys. A* **802**, 67 (2008).  
 [24] A. Gómez Camacho *et al.*, *Nucl. Phys. A* **833**, 156 (2010).  
 [25] F. A. Souza *et al.*, *Phys. Rev. C* **75**, 044601 (2007).  
 [26] H. Kumawat *et al.*, *Phys. Rev. C* **78**, 044617 (2008).  
 [27] A. M. M. Maciel *et al.*, *Phys. Rev. C* **59**, 2103 (1999).  
 [28] J. Lubian *et al.*, *Phys. Rev. C* **64**, 027601 (2001).  
 [29] J. Lubian *et al.*, *Nucl. Phys. A* **791**, 24 (2007).  
 [30] A. R. Garcia *et al.*, *Phys. Rev. C* **76**, 067603 (2007).  
 [31] J. Lubian *et al.*, *Phys. Rev. C* **79**, 064605 (2009).  
 [32] A. Gómez Camacho, P. R. S. Gomes, J. Lubian, and I. Padron, *Phys. Rev. C* **77**, 054606 (2008).  
 [33] A. Gómez Camacho, E. F. Aguilera, and A. M. Moro, *Nucl. Phys. A* **762**, 216 (2005).  
 [34] J. E. Poling, E. Norbeck, and R. R. Carlson, *Phys. Rev. C* **13**, 648 (1976).  
 [35] J. Cook, *Nucl. Phys. A* **375**, 238 (1982).  
 [36] M. F. Vineyard, J. Cook, and K. W. Kemper, *Nucl. Phys. A* **405**, 429 (1983).  
 [37] M. Sinha *et al.*, *Eur. Phys. J. A* **44**, 403 (2010).  
 [38] A. Pakou *et al.*, preprint NPL08\_1 [<http://www.uoi.gr/physics/npl/preprints.htm>].  
 [39] M. Sinha *et al.*, *Phys. Rev. C* **76**, 027603 (2007).  
 [40] M. Sinha *et al.*, *Phys. Rev. C* **78**, 027601 (2008).  
 [41] C. Y. Wong, *Phys. Rev. Lett.* **31**, 766 (1973).  
 [42] K. Zerva *et al.*, *Phys. Rev. C* **82**, 044607 (2010).